Tight-binding study of quantum transport in nanoscale GaAs Schottky MOSFET

Zahra Ahangari[a)†] and Morteza Fathipour[b)]

[a)] *Department of Electrical Engineering, Science and Research Branch, Islamic Azad University, Tehran, Iran*
[b)] *School of Electrical and Computer Engineering, University of Tehran, Tehran, Iran*

(Received 4 January 2013; revised manuscript received 20 April 2013)

This paper explores the band structure effect to elucidate the feasibility of an ultra-scaled GaAs Schottky MOSFET (SBFET) in a nanoscale regime. We have employed a 20-band $sp^3d^5s^*$ tight-binding (TB) approach to compute $E-K$ dispersion. The considerable difference between the extracted effective masses from the TB approach and bulk values implies that quantum confinement affects the device performance. Beside high injection velocity, the ultra-scaled GaAs SBFET suffers from a low conduction band DOS in the Γ valley that results in serious degradation of the gate capacitance. Quantum confinement also results in an increment of the effective Schottky barrier height (SBH). Enhanced Schottky barriers form a double barrier potential well along the channel that leads to resonant tunneling and alters the normal operation of the SBFET. Major factors that may lead to resonant tunneling are investigated. Resonant tunneling occurs at low temperatures and low drain voltages, and gradually diminishes as the channel thickness and the gate length scale down. Accordingly, the GaAs (100) SBFET has poor ballistic performance in nanoscale regime.

Keywords: band structure, quantum confinement effects, resonant tunneling, Schottky MOSFET

PACS: 85.30.Tv, 73.30.+y, 73.61.Ey, 31.15.aq **DOI:** 10.1088/1674-1056/22/9/098502

1. Introduction

An aggressively scaled conventional MOSFET suffers from a high series resistance of the ultra-thin source/drain junctions that significantly degrades the device performance. The Schottky barrier source/drain MOSFET (SBFET) has beem introduced as an alternative structure that can overcome scaling problem issues and effectively eliminates parasitic source/drain resistance.[1–4] On the other hand, high mobility channel materials such as III–V semiconductors have been explored for high-performance MOSFETs. New-found process technologies such as atomic layer deposition and usage of high-k dielectrics for the gate insulator allows the application of III–V semiconductors as the channel material in order to benefit from its high mobility for yielding enhanced on-current.[5–9] We have, for the first time, combined the advantages of high mobility GaAs and the low parasitic resistance of an SBFET to explore quantum transport of a GaAs SBFET and have clarified the feasibility of this device in the nanoscale regime. In order to improve the on-state current in the SBFET, the Schottky barrier height (SBH) at the source/drain must be lowered (< 0.1 eV).[4] Unfortunately, the SBH is independent of the metal source/drain work function as a result of Fermi level pinning.[10] In Ref. [10], a technique is introduced in which the pinned Fermi level of metal/n-GaAs shifts towards the conduction band that leads to a considerable reduction of SBH by insertion of a thin insulator between the metal and GaAs.

In this paper, we thoroughly investigate the quantum confinement effect on the ballistic performance of a GaAs SBFET. The effective mass approach may not predict the quantization effects in an ultra-thin body (UTB) accurately.[7,8,11] A precise treatment of the full band structure is used by applying a 20 orbital $sp^3d^5s^*$ tight binding approach in the SBFET. Quantum confinement increases the energy level of subbands. Subband energy level enhancement increases the effective SBH. In this situation, Schottky barriers at the source/drain and channel form a double barrier profile along the transport direction. Since tunneling is the main current component in an SBFET, resonant tunneling may occur. We have conducted a comprehensive study to examine several factors such as bias voltage, temperature (T), gate length (L_G), and channel thickness (T_{ch}) responsible for the occurrence of resonant tunneling. Resonant tunneling changes the normal performance of an SBFET.

The paper is organized as follows. Section 2 discusses the quantum confinement effect in UTB structure in depth and calculates in-plane and confinement effective masses as a function of number of atomic layers. In Section 3, the performance of the ultra scaled SBFET is investigated and a simulation approach based on the non-equilibrium Green's function (NEGF) formalism is presented. Section 4 explores the possibility of resonant tunneling in an SBFET. Section 5 summarizes the paper.

[†]Corresponding author. E-mail: z.ahangari@iausr.ac.ir

2. Exploring the quantum confinement effect on the band structure of a UTB GaAs SBFET

The double-gate UTB SBFET (100)/[100] is depicted in the inset in Fig. 1. We have employed a nearest-neighbor $sp^3d^5s^*$ tight-binding approach for calculating the band structure in the UTB SBFET. Passivation of the surface dangling bonds is applied in the UTB Hamiltonian. Tight binding parameters that are extracted from Ref. [12] result in accurate values for the band gap and effective masses in both conduction and valence bands.

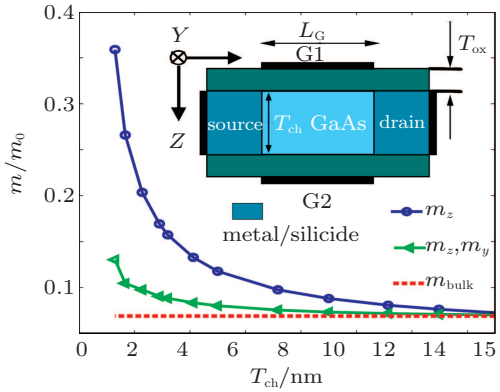

Fig. 1. (color online) Confinement (m_z) and in-plane effective mass (m_x, m_y) of the Γ valley as a function of channel thickness. Inset: double-gate SOI MOSFET with metal source/drain.

Figure 1 presents the extracted confinement (m_z) and in-plane effective mass (m_x, m_y) of the Γ valley as a function of channel thickness. The confinement effective mass increases significantly due to size quantization. In-plane effective mass is calculated by fitting a parabola dispersion at the minimum of the conduction band at the Γ point. The confinement effective mass is deduced from the energy difference between the minimum value of conduction band in bulk band structure and the lowest subband located at the Γ point that is calculated by tight binding approach. The change in the confinement and in-plane effective mass of the UTB SBFET results in a considerable distinction in the effective SBH, injection velocity, tunneling probability, and current in comparison to the case where bulk effective masses are used.

Figures 2(a)–2(c) illustrates the $E-K$ dispersion relation of thin film GaAs as the channel thickness shrinks from 5 nm down to about 1.67 nm (11 atomic layer). For T_{ch}=5 nm, subbands from the Γ valley have the lowest energy. Γ–L energy split is 0.24 eV. As the thickness of channel scales down to 3 nm, the energy difference between Γ–L reduces to 0.222 eV and the minimum energy still appears at the Γ point. Subbands from the Γ valley play an important role in the transport. These subbands provide high injection velocity due to low in-plane effective mass. Furthermore, low transport effective mass increases the tunneling probability. On the other hand, the light effective mass of the Γ valley leads to a smaller density of states (DOS) and lower gate capacitance (C_G). For the ultra-scaled structure, $T_{ch} = 1.67$ nm, the energy separation between Γ and four L valleys is reduced to 0.18 eV. Γ is the dominant valley in the transport for the UTB SBFET until the L valleys begin to conduct under strong inversion and higher gate voltages.

Figure 2(d) presents the lowest subband energy of an ultra-scaled GaAs SBFET for approximately $T_{ch} = 1.67$ nm within the two-dimensional (2D) Brillouin zone. The minimum energy occurs at the Γ point ($k_x = k_y = 0$). Due to size quantization, the energy of the band gap increases by the difference $1.9 - 1.42 = 0.48$ eV, compared with the related bulk value (1.42 eV).

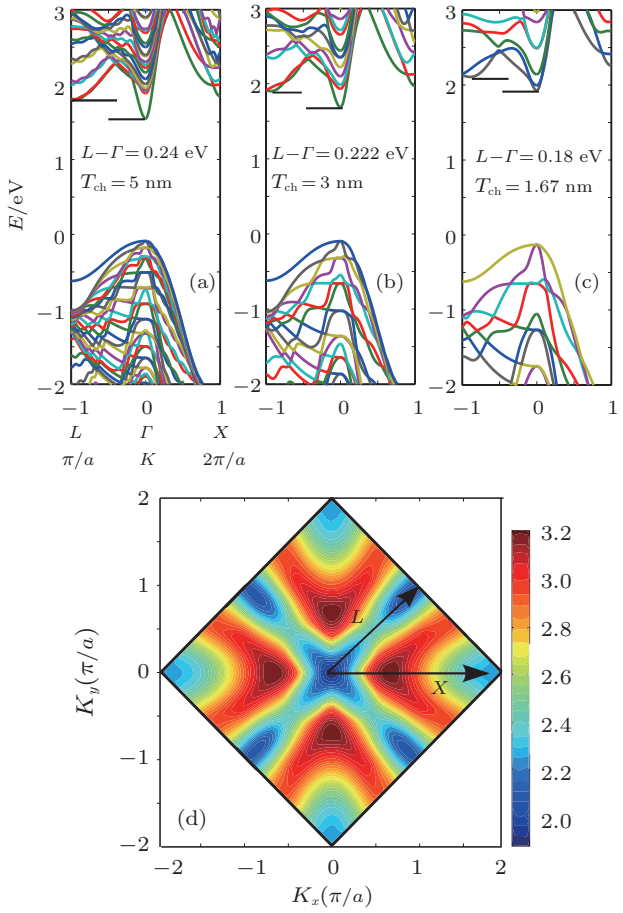

Fig. 2. (color online) (a)–(c) Band structure as a function of thin film thickness. (d) Lowest subband of GaAs SBFET for approximately $T_{ch} = 1.67$ nm within the 2D Brillouin zone.

3. Performance assessment of the GaAs SBFET

The gate capacitance C_G that has a significant role in the performance of the SBFET is a series combination of gate oxide capacitance (C_{ox}) and quantum (semiconductor) capacitance (C_Q). The C_Q is a function of the DOS in the channel. The 2D DOS is calculated as a function of channel thickness for GaAs(100) and UTB Si(100), and $T_{ch} = 1.73$ nm. The results are presented in Fig. 3. The UTB Si(100) has a higher DOS than GaAs. In the thick GaAs channel structure, due to multiple energy state occupation, C_Q is higher than that of ultra-thin bodies.

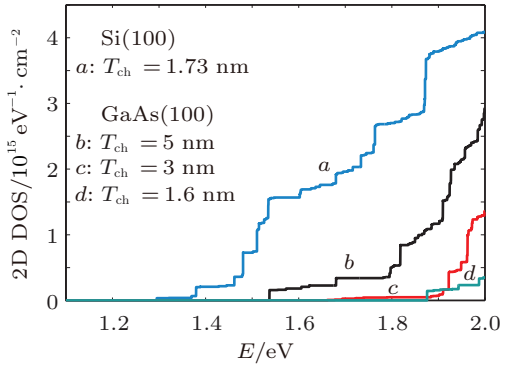

Fig. 3. (color online) The 2D DOS for different channel thicknesses of GaAs(100) and UTB Si(100).

Constant $C_{ox} = 3.4$ μF/cm^2 is considered in our study for elucidating the impact of size quantization on C_Q. For $T_{ch} = 5$ nm, the gate coupling over the channel is not significantly strong and C_Q is 2.41 μF/cm^2. Shrinking the channel thickness to 3 nm where the impact of size quantization on DOS and C_Q is not dominant, leads to a better gate coupling to the body region. Tunneling is indeed a dominant current component of an SBFET and strongly depends upon SBH and Schottky barrier width. The effect of scaling down the channel thickness on improvement of current injection is intuitive and accordingly results in a larger probability of tunneling through the barriers. Further shrinking the channel thickness ($T_{ch} = 1.67$ nm) enhances the energy of the lowest subband. In an ultimately scaled SBFET, due to lack of DOS in the Γ valley, C_Q is decreased to 1.58 μF/cm^2. Hence, C_Q has outstanding effect on the overall gate capacitance especially if the gate insulator is very thin. As a result, in an ultimately scaled (100) GaAs SBFET, size quantization degrades the device performance and therefore diminishes better gate coupling over the channel.

The lowest subband profile along the channel is calculated as the channel thickness scales down from 5 nm to 1.67 nm (Γ and L valleys) by solving self-consistent 2D Schrödinger–Poisson equations in the channel, as depicted in Fig. 4(a). Gate voltage (V_{GS}) and drain voltage (V_{DS}) are set to be $V_{GS} = V_{DS}$ =0.4 V determined by ITRS suitable for devices having low power and high performance digital applications between 2013 and 2016.[13] To clarify the performance of the GaAs SBFET, we have restricted our simulation to SBH = 0.1 eV.[4] Due to strong confinement in the depth of the channel, the energy of the first allowed subband increases.[14–17] The effective SBHs in the lowest suband of the Γ valley are approximately 0.12, 0.22, and 0.41 eV higher than initially defined SBH for $T_{ch} = 5$, 3, and 1.67 nm, respectively. This effect is more pronounced for the UTB GaAs SBFET ($T_{ch} = 1.67$ nm) in the Γ and L valleys.

The ballistic I_D–V_{GS} characteristic is calculated by using the NEGF[18–21] approach as a function of channel thickness using thickness-dependent effective masses. The results are illustrated in Fig. 4(b). For each individual channel thickness, however, it is essential to compute the band structure and extract the effective masses in three directions (m_x, m_y, m_z). The first one-dimensional (1D) Schrödinger equation is solved in each slice along the transverse direction at each mesh grid along the channel,

$$\left[-\frac{\hbar^2}{2m_z^*}\frac{\partial^2}{\partial z^2} + U(x,z)\right]\psi(x,z) = E_z(x)\psi(x,z), \tag{1}$$

where $E_z(x)$ is the eigen energy or vertical mode, $\psi(x,z)$ is the eigenfunction in the vertical direction at each x grid, and $U(x,z)$ is the potential in each slice along the transverse direction.

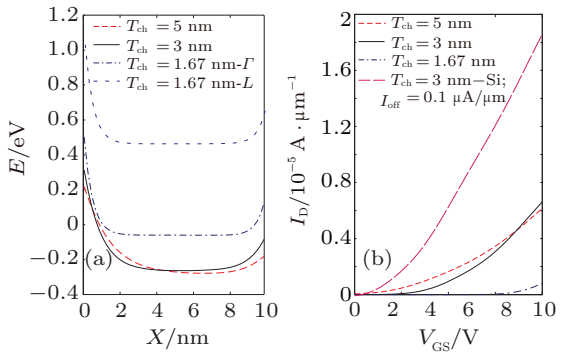

Fig. 4. (color online) (a) First subband profile along the channel for SBH = 0.1 eV as the channel thickness scales down from 5 nm to 1.67 nm for $V_{DS} = V_{GS} = 0.4$ V and $L_G = 10$ nm. (b) Curves of I_D–V_{GS} for different channel thicknesses.

For calculating current by using the NEGF formalism, the 1D Schrödinger equation must be solved with an open boundary condition along the transport direction. The vertical mode energy is considered as the potential energy along the channel.

$$\left[\frac{-\hbar^2}{2m_x^*}\frac{\partial^2}{\partial x^2} + E_z(x)\right]\phi_i(x) = E_L(x)\phi_i(x), \tag{2}$$

where H_x is defined as

$$H_x = \left[\frac{-\hbar^2}{2m_x^*}\frac{\partial^2}{\partial x^2} + E_z(x)\right], \tag{3}$$

where $E_L(x)$ is the eigen energy, and $\phi_i(x)$ is the eigenfunction along the x direction. The transmission coefficient for energies in the transport direction, $T(E_L)$, must be calculated as follows:[18]

$$T(E_L) = \mathrm{trace}\left(\Gamma_S G \Gamma_D G^\dagger\right), \tag{4}$$

where

$$G = \left[E_L(x)I - H_x - \Sigma_S - \Sigma_D\right]^{-1}. \tag{5}$$

In the above equations, $\Sigma_{S,D}$ are the self-energy denoting the coupling between channel and the source/drain reservoirs, G is the retarded Green's function, and Γ is the imaginary part of the self energy denoting the broadening function. Total current for the coherent transport is calculated as follows:

$$I_{DS} = \frac{2q}{h}\int \mathrm{d}E_L T(E_L)\left[F_{-1/2}(E_{FS} - E_L)\right.$$

$$- F_{-1/2}(E_{\rm FD} - E_{\rm L})\big], \tag{6}$$

$$F_{-1/2}(\varepsilon) = \frac{1}{\sqrt{\pi}} \int_0^{\infty} \frac{t^{-1/2}\,{\rm d}t}{1+\exp(t-\varepsilon)}, \tag{7}$$

where F is the Fermi Dirac integral of the order $-1/2$, T denotes the lattice temperature, and $k_{\rm B}T$ is the Boltzmann constant. The $E_{\rm FS}$ and $E_{\rm FD}$ are the source and drain Fermi energies, respectively. Threshold voltage increases as the channel thickness decreases. Effect of quantum confinement is more observable for $T_{\rm ch}$=1.67 nm as the device suffers from the low carrier density in the Γ valley. Transport effective mass enhancement beside high effective SBHs reduces the tunneling probability and degrades its performance. For $T_{\rm ch}$=3 nm and $L_{\rm G}$=10 nm, $I_{\rm off}$ is set to be 0.1 μA/μm in GaAs SBFFET, according to ITRS. The $I_{\rm on}$ for a silicon-based MOSFET is 1500 μA/μm.[13] Enhanced Schottky barriers and a low DOS in GaAs SBFET degrades the performance of this device in comparison with a silicon-based channel.

4. Assessment of resonant tunneling in the GaAs SBFET

As implied in Section 3, quantum confinement increases the effective SBH. The results for the transmission coefficient versus energy for $T_{\rm ch} = 3$ nm and $L_{\rm G} = 10$ nm is plotted along the channel as a function of $V_{\rm DS}$ ranging from 0.05 to 0.4 V, illustrated in Fig. 5. For low drain voltages and due to high effective SBHs at the source/drain, a double barrier profile is created, resulting in the formation of resonant states along the channel. We have assessed whether the resonant tunneling effect can be observed in this device or not.

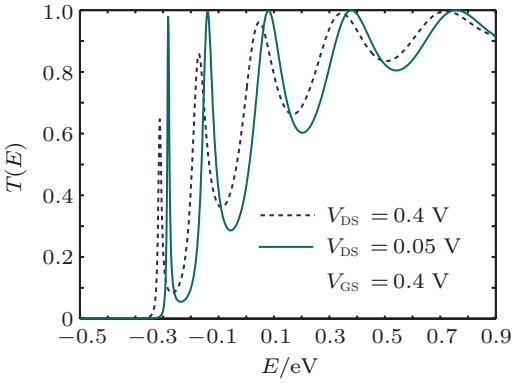

Fig. 5. (color online) Transmission versus energy for $V_{\rm GS} = 0.4$ V and $V_{\rm DS} = 0.05$ and 0.4 V.

Since the energy of electrons in the energy interval between $E_{\rm FS}$ and $E_{\rm FD}$ coincides with the energy of localized states in the channel, resonant tunneling appears. Transmission reflects the energy distribution of resonant states. For $V_{\rm DS}$=0.05 V, the electron transmission coefficient through the channel sharply peaks around certain energies. Hence, current propagates through discrete resonant states. As the drain voltage increases, the potential well curvature along the channel is gradually diminished and several states are involved in the current simultaneously. Accordingly, resonant tunneling is gently suppressed and direct tunneling makes the transmission increase slowly from zero to one.

The local electron density of states (LDOS) along the channel is presented in Fig. 6, where $V_{\rm GS} = 0.4$ V and $V_{\rm DS} = 0.05$ V. The bright regions imply that the probability of existence of electrons is high. It is evident that the double barrier profile in the channel acts as a quantum well. The energy split between resonant states varies as the gate voltage increases and effectively raises the number of resonant states that can drive the current. In addition, for distinguishable resonant tunneling, $V_{\rm DS}$ must be smaller than the energy separation of adjacent resonant states.

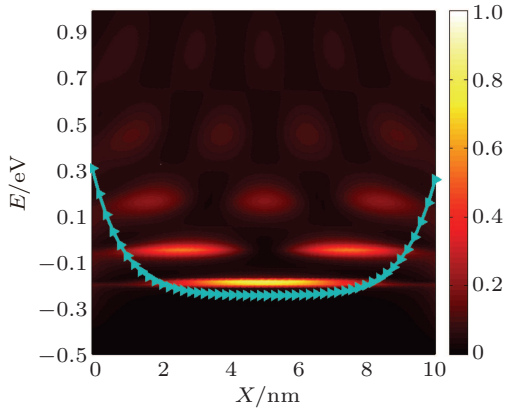

Fig. 6. (color online) Local electron density of states (LDOS) and first subband profile along the channel at $V_{\rm GS} = 0.4$ V and $V_{\rm DS} = 0.05$ V. Bright regions indicate higher density of states; dark regions indicate lower density of states.

For clarifying resonant tunneling and its impact on the electrical characteristic of SBFET, essential factors such as bias voltage, temperature, channel thickness, and gate length are taken into account.

The role of temperature on the performance of SBFET is investigated as a function of channel thickness for $L_{\rm G} = 10$ nm (see Fig. 7). $V_{\rm DS}$ is considered to be 0.05 V to make resonant tunneling through discrete resonant states visible. Thermal energy is 6.6 meV at $T = 77$ K and increases to 25 meV at room temperature. Resonant tunneling is apparent for $T_{\rm ch} = 5$ nm and $T_{\rm ch} = 3$ nm at low temperatures and the negative differential resistance region appears in the transfer characteristic. As the temperature increases, resonant tunneling gradually disappears and only current oscillation occurs in the transfer characteristic. This effect is due to thermal energy broadening of carriers which influences DOS, transmission, and current. Multiple resonant states contribute to resonant tunneling for $T_{\rm ch} = 3$ nm and $T_{\rm ch} = 5$ nm. Peak to valley ratio (PVR) for $T_{\rm ch} = 5$ nm is higher than $T_{\rm ch} = 3$ nm due to higher energy spacing between adjacent resonant states. For extremely scaled SBFET ($T_{\rm ch} = 1.67$ nm), the energy of the first resonant state raises. In this situation, only a small portion of electrons with higher energy are involved in resonant tunneling through

the first resonant state. Hence, no prominent peak or valley is distinguishable in the transfer characteristic as the temperature changes from $T = 77$ K to room temperature.

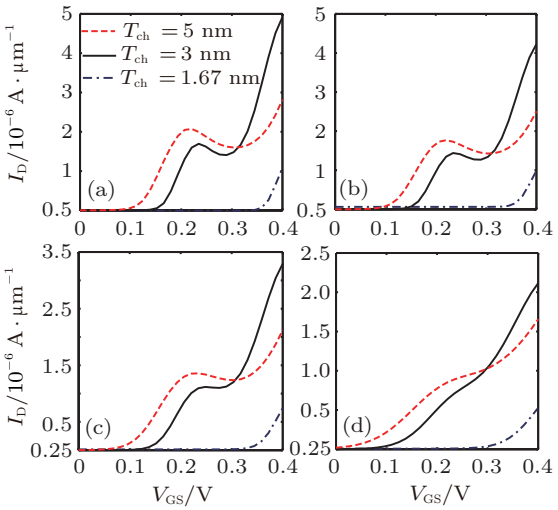

Fig. 7. (color online) I_D–V_{GS} for different channel thicknesses at $V_{DS} = 0.05$ V and $L_G = 10$ nm: (a) $T = 77$ K, (b) $T = 100$ K, (c) $T = 150$ K, and (d) $T = 300$ K.

The V_{DS} has a key role in the shape of the potential well along the channel. For high enough V_{DS}, the curvature of the quantum well channel is completely diminished. In this situation, the carriers are free of any confinement in the transport direction (x). Figure 8 illustrates the impact of V_{DS} on the transfer characteristic of the SBFET at $T = 77$ K as V_{DS} ranges from 0.02 to 0.15 V as a function of channel thickness. For $V_{DS} = 0.02$ V, resonant tunneling is distinguishable for $T_{ch} = 3$ nm and $T_{ch} = 5$ nm. As V_{DS} increases to 0.15 V, multiple resonant states contribute to the current and the resonant tunneling is gradually diminished.

It is essential to consider the role of aggressive gate length scaling that will help identify the effect of resonant tunneling more accurately. The results are presented in Fig. 9 for $L_G = 10$, 8, and 6 nm as a function of channel thickness for $T = 77$ K and $V_{DS} = 0.05$ V. As the gate length scales down, the Schottky barriers strongly affect the double barrier profile

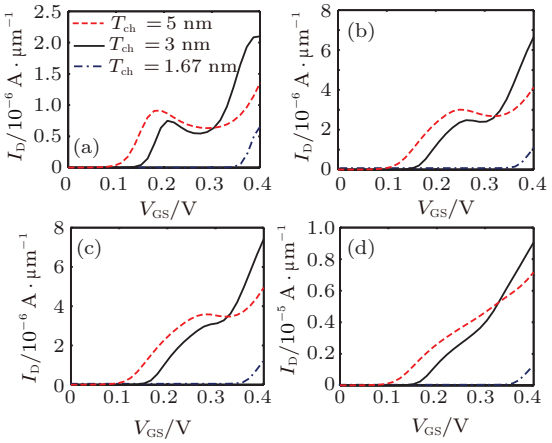

Fig. 8. (color online) I_D–V_{GS} curves for different channel thicknesses at $T = 77$ K and $L_G = 10$ nm: (a) $V_{DS} = 0.02$ V, (b) $V_{DS} = 0.08$ V, (c) $V_{DS} = 0.1$ V, and (d) $V_{DS} = 0.15$ V.

and form a parabolic potential along the transport direction. The energy separation between consecutive resonant states is inversely proportional to gate length. If the subband is constrained in the longitudinal direction, the resonant states within the subband will react to this confinement by increasing in energy. Transconductance (gm) is calculated to clarify resonant tunneling. Negative gm implies the occurrence of resonant tunneling. The C_G and gate length determine the number of resonant states that contribute to current. With the reduction of channel thickness to 3 nm, the energy split of resonant states decreases. Simulation results indicate that PVR and resonant tunneling phenomena sensitively depend upon the gate length and C_G.

For $T_{ch} = 3$ nm and $T_{ch} = 5$ nm in the case of $L_G = 10$ nm, two lowest resonant states contribute to current and resonant peaks are distinctly separated. For $L_G = 8$ nm, resonant tunneling is distinguishable and PVR is enhanced compared with $L_G = 10$ nm. As the gate length scales down to 6 nm, the second resonant state is enhanced in energy and direct tunneling occurs only through the first resonant state from source to drain. There is no evidence of resonant tunneling in the transfer characteristic. Positive gm for $L_G = 6$ nm confirms

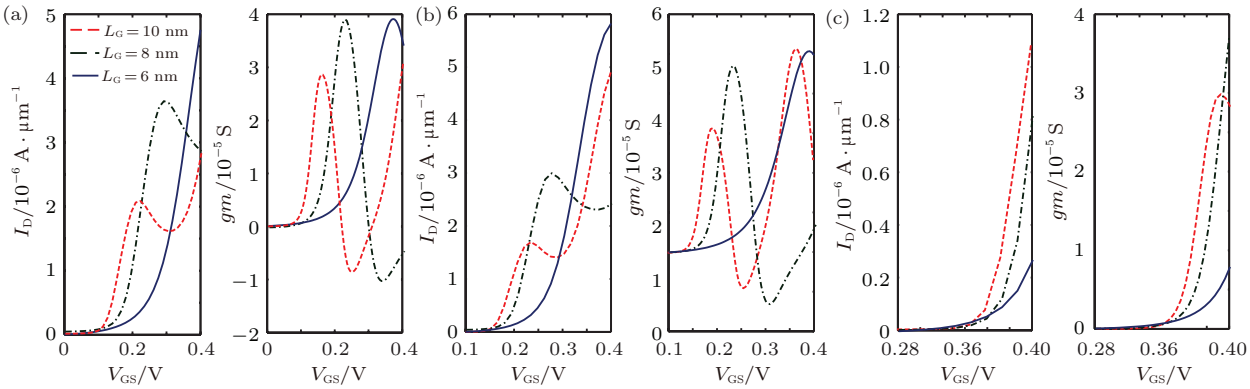

Fig. 9. (color online) I_D–V_{GS} and gm in gate length range from 10 to 6 nm for $V_{GS} = 0.4$ V, $V_{DS} = 0.05$ V, and $T = 77$ K. (a) $T_{ch} = 5$ nm, (b) $T_{ch} = 3$ nm, and (c) $T_{ch} = 1.67$ nm.

direct tunneling from source to drain. For an ultra scaled structure, $T_{ch} = 1.67$ nm, lack of DOS results in dominant role of C_Q on C_G. Carriers with higher energy are involved with direct tunneling through the lower energy state. Tunneling probability lowers as the gate length reduces to 6 nm which allows the poor ballistic performance of the GaAs SBFET in the nanoscale regime. Resonant tunneling changes the common performance of SBFETs. Structural parameters definitely affect resonant tunneling. PVR increases as the gate length scales down but a further scaling of the gate length results in replacement of direct tunneling instead of resonant tunneling. Resonant tunneling is gradually smoothed out as the channel thickness and gate length shrink down simultaneously for a low SBH.

In conclusion, resonant tunneling occurs under certain conditions and changes to direct tunneling in ultra-scaled structures. Simulation results reveal that resonant tunneling sensitively depends upon the gate length and C_G. Resonant tunneling occurs when the subband can be modulated by C_G and form a potential well along the channel. In an ultra-scaled structure, the decrease in C_G results in direct tunneling of the carriers through the lower energy state. By scaling down the gate length, the energy states increase in energy. The Schottky barriers at the source/drain pull the channel potential towards each other and form a parabolic potential profile along the channel. Resonant tunneling is gradually diminished as the energy of resonant states increases. The above discussion is illustrated in Fig. 10.

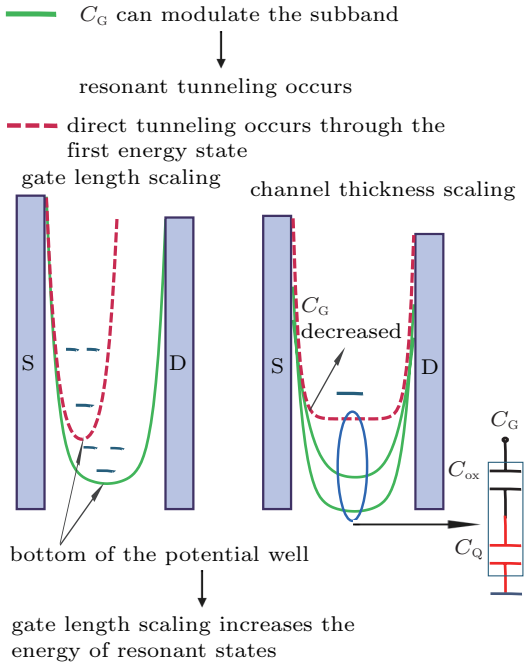

Fig. 10. (color online) Schematic of conditions for the occurrence of resonant and direct tunneling in the GaAs SBFET at low temperatures and low drain voltages.

5. Conclusion

We have studied the quantum transport of a UTB GaAs SBFET to elucidate the ultimate performance and feasibility of this device in the nanoscale regime, employing an $sp^3d^5s^*$ tight binding approach. Quantum confinement affects the band structure and accordingly increases the effective masses from their bulk value that significantly changes the electrical performance of the GaAs SBFET. Beside high injection velocity, the ultimately scaled GaAs SBFET suffers from a lack of DOS and consequently has a small quantum capacitance in the Γ valley that degrades the overall gate capacitance. Size quantization increases the energy level of subbands and results in the effective SBH enhancement. Schottky barriers at the source/drain form a double barrier profile along the channel that result in resonant tunneling under certain conditions. Resonant tunneling changes the normal performance of an SBFET and depends considerably upon temperature and drain voltage. As the channel thickness and gate length scale down, resonant tunneling is gradually diminished. Finally, beside high injection velocity, the (100) GaAs SBFET has poor electrical performance in the nanoscale regime.

References

[1] Xiong S, King T J and Bokor J 2005 *IEEE Trans. Electron Dev.* **52** 1859
[2] Vega R A 2006 *IEEE Trans. Electron Dev.* **53** 866
[3] Nishi Y, Kinoshita A, Hagishima D and Koga J 2008 *Jpn. J. Appl. Phys.* **47** 99
[4] Larson J M and Snyder J P 2006 *IEEE Trans. Electron Dev.* **53** 1048
[5] Luisier M 2011 *IEEE Trans. Electron Dev. Lett.* **32** 1686
[6] Kim R, Rakshit T, Kotlyar R, Hasan S and Weber C E 2011 *IEEE Trans. Electron Dev. Lett.* **32** 746
[7] Guan X, Lu J, Wang Y and Yu Z 2006 *Proceeding of International Conference on Simulation of Semiconductor Processes and Devices* p. 248
[8] Yang L, Neophytou N, Klimeck G and Lundstrom M S 2008 *IEEE Trans. Electron Dev.* **55** 1116
[9] Seung H P, Yang L, Kharche N, Jelodar M S, Klimeck G, Lundstrom M S and Luisier M 2012 *IEEE Trans. Electron Dev. Lett.* **59** 2107
[10] Hu J, Saraswat K C and Philip Wong H S 2010 *J. Appl. Phys.* **107** 063712
[11] Zhu Z G, Low T, Li M F, Fan W J, Bai P, Kwong D L and Samudra G 2008 *Semicond. Sci. Technol.* **23** 025009
[12] Boykin T B, Klimeck G, Bowen R C and Oyafuso F 2002 *Phys. Rev. B* **66** 125207
[13] International Technology Roadmap for Semiconductors
[14] Guo J and Lundstrom M S 2002 *IEEE Trans. Electron Dev.* **49** 1897
[15] Afzalian A and Flandre D 2011 *Solid State Electronics.* **65** 123
[16] Toriyama S 2010 *Jpn. J. Appl. Phys.* **49** 104204
[17] Luan S Z and Liu H X 2008 *Chin. Phys. B* **17** 3077
[18] Datta S 2005 *Quantum Transport: Atom to Transistor* (Cambridge: Cambridge University Press)
[19] Shin M 2010 *Appl. Phys. Lett.* **97** 092108
[20] Venugopal R, Ren Z, Datta S, Lundstrom M S and Jovanovic D 2002 *J. Appl. Phys.* **92** 3730
[21] Ren Z, Venugopal R, Goasguen S and Datta S 2003 *IEEE Trans. Electron Dev.* **50** 1914